Chinese Chemical Letters 37 (2026) 111195

Contents lists available at ScienceDirect

Chinese Chemical Letters

journal homepage: www.elsevier.com/locate/cclet

NIR light-activated programmable drug immobilization and oxygen modulation for enhanced photodynamic and chemo-therapy

Yu Si[a], Xueying Jiang[a], Zhigang Gao[a], Yuan Liang[b,*], Wen Sun[a], Engin U. Akkaya[a], Lei Wang[a,*]

[a] Cancer Hospital of Dalian University of Technology, Department of Pharmaceutical Engineering, Dalian University of Technology, Dalian 116024, China
[b] Department of Thoracic Oncology, Cancer Hospital of Dalian University of Technology, Liaoning Cancer Hospital & Institute, Shenyang 110042, China

ARTICLE INFO

Article history:
Received 11 February 2025
Revised 3 April 2025
Accepted 9 April 2025
Available online 16 April 2025

Keywords:
BODIPY
Photochemistry
Near-infrared light
Photodynamic therapy
Synergistic cancer therapy

ABSTRACT

Photodynamic therapy (PDT) has attracted various attentions for cancer treatment, yet current strategies suffer many limitations including short retention time of photosensitizers, exacerbation of hypoxia due to oxygen consumption and restricted release of singlet oxygen under hypoxic conditions or in the absence of light. We present here a promising cancer therapy which not only reduces the frequency of drug administration and overall drug dosage through near-infrared (NIR) light-triggered drug immobilization in tumor sites, but also enhances anticancer efficacy by synergistic treatments through PDT and chemotherapeutic drug camptothecin. More importantly, endoperoxides generated *in situ* can not only persistently release singlet oxygen even in the absence of light, thereby augmenting PDT efficacy, but also release triplet oxygen to alleviate tumor hypoxia exacerbated by PDT. Its enhanced retention time was demonstrated both *in vitro* (96 h) and *in vivo* (240 h), with the duration adjustable by varying the light source. Notably, a single administration (3 mg/mL, 300 μL) during the entire treatment under low-power red light irradiation (11 mW/cm^2) resulted in efficient suppression of the tumor growth and pulmonary metastasis. This NIR light-triggered long-acting platforms could be utilized for design of long-term disease imaging and therapy tools, and the *in situ* generated endoperoxide is promising for self-regulation of tumor hypoxia.

© 2025 Published by Elsevier B.V. on behalf of Chinese Chemical Society and Institute of Materia Medica, Chinese Academy of Medical Sciences.

Photodynamic therapy (PDT) has attracted considerable attention as a promising modality for cancer treatment due to its low side effects, high specificity and minimal invasiveness [1,2]. Under light irradiation, photosensitizers (PSs) can transfer absorbed energy to afford reactive oxygen species (ROS), especially singlet oxygen ($^1O_2$) which directly kill cancer cells, damage the blood vessels in tumors and elicit the immune responses to eliminate cancer cells. As singlet oxygen has a brief lifetime and a restricted diffusion radius, the photodamage induced by the PSs is confined to its immediate surroundings in the presence of light exposure. Therefore, the effectiveness of photodynamic therapy is highly reliant on the intracellular accumulation and retention of the PSs in tumor site. However, most photosensitizers are quickly cleared from the bloodstream within hours and could not accumulate at tumor sites [3], which commonly resulting repetitive injections and leading to overdose of PSs in body. Despite of the low toxicity of PSs, large dosing in normal tissue may cause fever or systemic side effects [4]. Due to the enhanced permeability and retention (EPR) effect, nanodrugs [5,6] can passively accumulate in tumors, markedly decreasing the clearance rate and prolonging the therapeutic time of small molecules. To date, an increasing number of PSs-involved nanodrugs [7,8] have been developed, including organic polymeric nanoparticles, inorganic materials, liposomes, peptide or protein-based nanomaterials. Despite their success, the reported PSs-involved nanodrugs mainly rely on the non-covalent interactions of nanomaterials with tumor site, which can be easily eliminated and repetitive injections for enhanced anticancer performance cannot be avoided [9]. Meanwhile, because of the complexity and various self-assembling pathways, design of self-assembling nanodrugs with controllability and tunability is challenging. Therefore, there is an urgent need for more efficient long-acting PDT nanodrugs that can eliminate tumors with reduced administration frequency and drug dosage, especially the one featuring controllability and tunability.

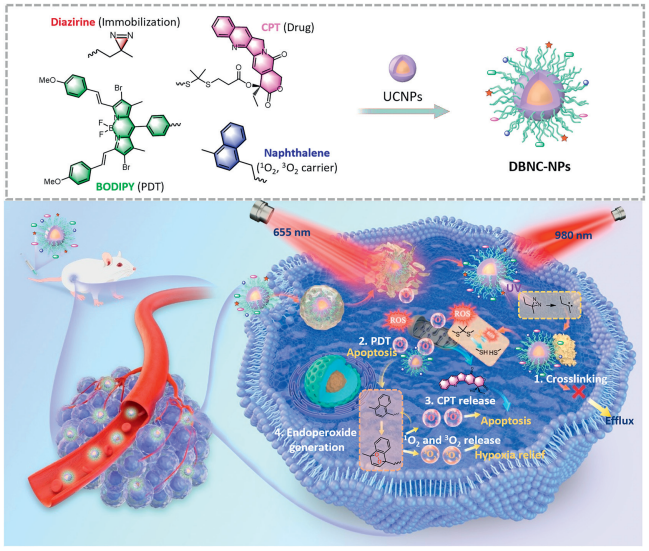
Another limitation of current PDT is the oxygen-deficient (hypoxic) tumor microenvironment [10] which present in the

* Corresponding authors.
E-mail addresses: liangyuan@cancer-hosp-ln-cmu.com (Y. Liang), leiwang@dlut.edu.cn (L. Wang).

https://doi.org/10.1016/j.cclet.2025.111195
1001-8417/© 2025 Published by Elsevier B.V. on behalf of Chinese Chemical Society and Institute of Materia Medica, Chinese Academy of Medical Sciences.

majority of solid tumors significantly limiting the efficacy of PDT as oxygen is critical to the process of photodynamic cell toxicity. More seriously, oxygens are rapidly consumed in traditional PDT, thus exacerbating hypoxia in the tumor. The increased expression of hypoxia-inducible factor 1α (HIF-1α) is strongly linked to tumor aggressiveness and resistance to treatment [11]. To address this, directly oxygen-delivery [12,13] or *in situ* oxygen production systems [14,15] have been developed. However, these strategies face significant challenges due to the complex synthesis processes, bio-compatibility concerns, safety risks and issues in drug delivery synergy. Recently, our group [16–18] and others [19–21] have demonstrated that endoperoxides, singlet oxygen carriers constructed *via in vitro* PDT, are potential anticancer agents which can self-deliver singlet oxygen to tumors through cycloreversion reaction without the need of oxygen in tumor. Interestingly, many endoperoxides can also liberate triplet oxygen [22] along with singlet oxygen, which may help alleviate tumor hypoxia and positively influence tumor behavior and response to treatments. Thus, PSs collaborated with endoperoxides could not only maintain $^1O_2$ generation in dark conditions which cannot be achieved in traditional PDT, but also transport triplet oxygen into tumor for relief hypoxia exacerbated by PDT. Until now, this self-regulation for hypoxia has not been explored in PDT.

Carbenes [23,24] can readily cross-link with nearby biomolecules *via* C–H bonds with a rate constant (k) of $3.1 \times 10^9\ s^{-1}$ [25], and this characteristic renders carbenes as ideal reactive intermediates associated with chemical biology [26,27]. However, diazirines as carbenes precursor are typically induced by ultraviolet-visible (UV–vis) light which cannot penetrate into deep tissues [28], thus limiting their *in vivo* applications. Compared to UV light, near-infrared (NIR) light can penetrate tissue much more deeply, and NIR light-activated nanomaterials is especially appealing for precision medicine due to its controllability and tunability [29,30]. Keeping all these points in mind, in this work, we developed a NIR light-triggered *in situ* controllable immobilization, and programmable therapeutic oxygen nanodrugs **DBNC-NPs** (Scheme 1) by precise functionalization of upconversion nanoparticles with diazirine, boron dipyrromethene (BODIPY), naphthalene and camptothecin (CPT). This novel nanodrug enhances the efficacy of photodynamic therapy by controlled immobilization of photosensitizers in tumor tissues through NIR light-induced carbenes formation and crosslinking with nearby biomolecules, thus reducing the frequency of administration and overall drug dosage. Additionally, it addresses the hypoxia challenges in traditional PDT by generating endoperoxides *in situ*, which can self-release triplet oxygen and singlet oxygen as two therapeutic agents.



Scheme 1. The design of NIR light-triggered long-acting nanodrugs and their enhanced and sustainable photodynamic and chemo-therapy.

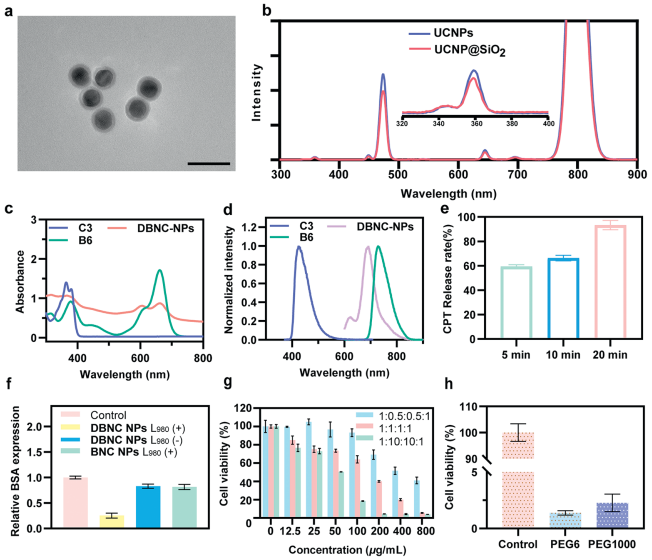


Fig. 1. (a) The representative TEM image of UCNP@SiO_2. Scale bar: 100 nm. (b) Fluorescence spectra of UCNPs (in hexane) and UCNP@SiO_2 (in ethanol) under 980 nm excitation. (c) The absorption spectrum of **C3** (200 μmol/L), **B6** (25 μmol/L) and **DBNC-NPs** (5 mg/mL) in *N*,*N*-dimethylformamide (DMF). (d) The normalized fluorescence of **C3** (200 μmol/L, $\lambda_{ex} = 367$ nm), **B6** (126 μmol/L, $\lambda_{ex} = 550$ nm) and **DBNC-NPs** (5 mg/mL, $\lambda_{ex} = 550$ nm) in DMF. (e) The CPT release with 655 nm light for 5, 10 or 20 min at an intensity of 10 mW/cm^2. (f) The relative BSA protein expression in supernatant after crosslinking shown in SDS-PAGE. BSA labeled by **DBNC-NPs** and **BNC-NPs** (1 mg/mL) with or without 980 nm laser irradiation. (g) Cell viability after PDT (655 nm, 10 mW/cm^2, 20 min) of **DBNC-NPs** composed of different molecule ratios. (h) Cell viability of nanodrugs with different PEG chains length after PDT (655 nm, 10 mW/cm^2, 20 min).

Upconversion nanoparticles (UCNPs) were synthesized using a previously established method [31], followed by coating with a silica shell (UCNP@SiO_2) to facilitate further surface modifications. Transmission electron microscopy (TEM) analysis revealed that the average diameters of the UCNPs and UCNP@SiO_2 were 33 ± 2 and 56 ± 4 nm, respectively (Fig. 1a and Fig. S1 in Supporting information), which is crucial for effective tumor retention as nanoparticles with a diameter between 30 nm and 200 nm can accumulate more effectively in tumor tissues [32]. This was further corroborated by dynamic light scattering (DLS) measurements, which showed hydrodynamic diameters of 44 and 68 nm for UCNPs and UCNP@SiO_2 (Fig. S2 in Supporting information). Moreover, UCNP@SiO_2 successfully emitted UV light when excited with a 980 nm laser, demonstrating its potential to activate photoreactive diazirine (Fig. 1b). Subsequent chemical modifications led to the preparation of amino-functionalized UCNPs, which were then used to construct **DBNC-NPs** (Scheme S4 in Supporting information). This process involved modifying the nanoparticles with various functional molecules including diazirine (**D2**), BODIPY (**B6**), naphthalene (**N1**) and CPT (**C3**) in a 1:10:10:1 molar ratio using a polyethylene glycol (PEG) linker (PEG6). All small molecules were synthesized *via* standard chemical strategies and were well characterized (see Supporting information). UV absorbance and fluorescence measurements confirmed the successful incorporation of these functional groups (Figs. 1c and d). The loading amount of BODIPY (**B6**) was determined by fluorescence, and the drug loading of BODIPY was calculated as 0.023 μmol/mg (Fig. S3 in Supporting information).

The thioketal linker in the **DBNC-NPs** was designed to be cleaved by reactive oxygen species generated during PDT [33], allowing for on-demand CPT release. To test the efficiency of thioketal linker response to ROS, **DBNC-NPs** was irradiated upon 655 nm light and the released CPT in was tested using UV–vis and high-performance liquid chromatography (HPLC). As shown in Fig. 1e and Fig. S4 (Supporting information), **DBNC-NPs** successfully released CPT under 655 nm light irradiation in a time-dependent manner, with approximately 90 % of free CPT detected after 20 min of irradiation (Fig. 1e). In addition, we selected bovine serum albumin (BSA) as a model to evaluate the photocrosslinking capability of **DBNC-NPs** toward proteins (Fig. 1f and Fig. S5 in Supporting information). BSA was firstly mixed with **DBNC-NPs** and **BNC-NPs** for 1 h and then exposed to a 980 nm laser light. After centrifugation, the supernatant was collected and analyzed *via* SDS-PAGE. It showed that weaker band was found in **DBNC-NPs** L_{980} (+) group but strong band in control groups, demonstrating that proteins were covalently labeled with **DBNC-NPs** under 980 nm laser irradiation.

Then, we studied the effect of molecule ratios and PEG length on anticancer performance. MTT assays for MCF-7 cells treated with **DBNC-NPs** loaded with various molecule ratios revealed that nanodrug with 1:10:10:1 molar ratio of **D2**, **B6**, **N1** and **C3** displayed the most potent anticancer effects, suggesting that BODIPY plays a crucial role in the anticancer mechanism (Fig. 1g). Next, **DBNC-NPs** with different PEG chain lengths (PEG6 and PEG1000) were prepared, and MTT assays indicated that PEG6-functionalized **DBNC-NPs** exhibited better PDT cytotoxicity (Fig. 1h) which was possible due to its higher molecules loading capacity [34,35]. Additionally, PEG6-functionalized **DBNC-NPs** displayed excellent water dispersibility which is crucial for subsequent biological studies (Fig. S6 in Supporting information).

With the optimal **DBNC-NPs** identified, we investigate its NIR light-induced long-acting performance in cell-based assays using fluorescence imaging. MCF-7 cells were incubated with **DBNC-NPs** or a control nanodrug **BNC-NPs** (without diazirine, Scheme S4) for 8 h, which were then irradiated by 980 nm light (Fig. 2a). As shown in Figs. 2b and c and Fig. S7 (Supporting information), strong red emissions were found from both two groups (indicated as 0 h), indicating that the nanodrugs successfully uptake into the cells. As anticipated, the fluorescence of control nanodrug **BNC-NPs** treated cells eliminated rapidly within 24 h, while **DBNC-NPs** treated group showed strong fluorescence even after 96 h. This sustained imaging ability suggests that the photo-crosslinked **DBNC-NPs** remained within the cancer cells, thus demonstrating the successful upconversion process, carbenes generation and the drug immobilization. Compared to previous long-acting strategies, our designed **DBNC-NPs** nanodrug features controllability and tunability as the crosslinking can be easily adjust by light exposure. To demonstrate this, intracellularly photo-induced crosslinking was examined. As shown in Figs. S8–S10 (Supporting information), the emission of **DBNC-NPs** in cells followed a light power density- and irradiation time-dependent manner, which strongly indicates its controllability and safety.

Next, the enhanced therapeutic property of **DBNC-NPs** proposed by NIR light-mediated photo-crosslinking was studied using MTT assays. The cells treated with **DBNC-NPs** were exposed with (L_{980+}) or without NIR light (L_{980-}) which were further incubated for 4 h. Under 655 nm red light irradiation for 20 min, two groups were incubated for 24 h allowing for MTT assays. As shown in Fig. 2d, the viabilities of the cells in two groups displayed significant difference and the NIR light irradiation caused more cell death, demonstrating the enhanced anticancer properties lead by crosslinking formation and the long-acting property. Encouraged by the excellent long-acting capability and enhanced therapeutic property of **DBNC-NPs** induced by NIR light, we further detailed

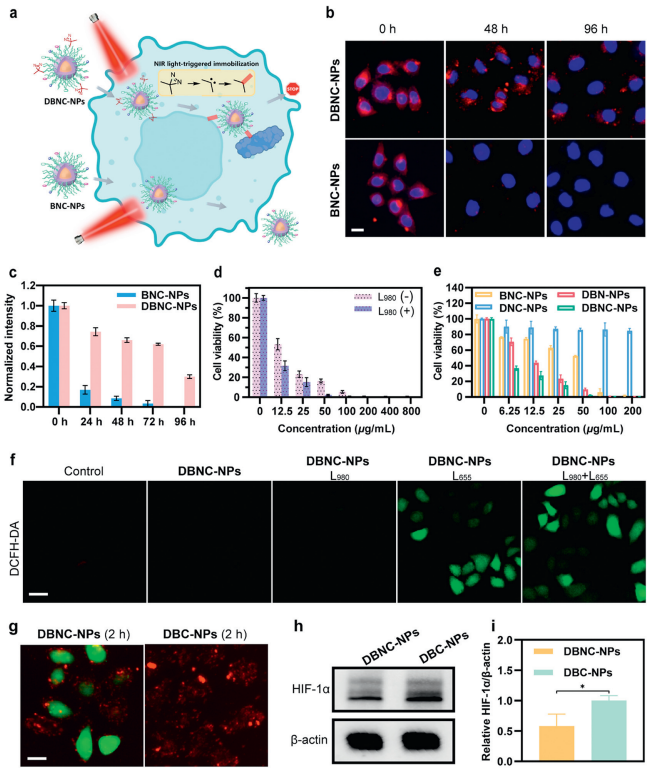


Fig. 2. (a) NIR light-induced long-acting performance of **BNC-NPs** and **DBNC-NPs** in MCF-7 cells. (b) Fluorescence imaging and (c) normalized fluorescent intensity of **BNC-NPs** (bottom) and **DBNC-NPs** (top) treated MCF-7 cells after 980 nm laser irradiation for crosslinking. Scale bar: 20 μm. (d) Cell viability of MCF-7 cells incubated with **DBNC-NPs** at various concentrations with or without 980 nm laser irradiation (3 W/cm^2, 4 min) followed 655 nm light irradiation (10 mW/cm^2 for 20 min). (e) Cell viability of MCF-7 cells incubated with **DBNC-NPs**, **BNC-NPs**, **DNC-NPs** and **DBN-NPs** at various concentrations under 980 nm and then 655 nm light irradiation. (f) Evaluation of $^1O_2$ generation in MCF-7 cells using DCFH-DA after different treatments. Scale bar: 20 μm. (g) $^1O_2$ generation in the dark, imaging was conducted after 2 h. Scale bar: 20 μm. (h, i) Western blot of HIF-1α of hypoxic cells under different treatments. Data are shown as mean ± SD ($n = 3$). $^*P < 0.05$.

the anticancer performance driven by different functional groups. Control nanodrugs including **BNC-NPs** (without diazirine), **DBN-NPs** (without CPT), **DNC-NPs** (without BODIPY) were prepared accordingly (Scheme S4). Their cytotoxicity toward MCF-7 cancer cells under 980 nm light-crosslinking and 655 nm light-PDT were tested using MTT assays. As shown in Fig. 2e, **DNC-NPs**, nanodrug without BODIPY showed no toxicity to cell under dual light irradiation, suggesting the importance of BODIPY for PDT [36]. **BNC-NPs** and **DBN-NPs** both showed inhibitory effect on cancer cells growth, owing the half maximal inhibitory concentration (IC_{50}) as 33.1 and 10.9 μg/mL, respectively. As expected, **DBNC-NPs** under 980 nm laser irradiation show the most promising PDT therapeutic properties to cancer cells and its IC_{50} was calculated as 4.2 μg/mL, which strongly suggesting the enhanced therapeutic property lead by photo-crosslinking and PDT/chemotherapy combination.

Encouraged by the enhanced anticancer performance of **DBNC-NPs**, we start to analyze the $^1O_2$ [37] released from **DBNC-NPs** during PDT, and 2,7-dichlorofluorescein diacetate (DCFH-DA) as a commonly used ROS probe was selected (Fig. 2f). As expected, negligible fluorescence was observed from the **DBNC-NPs** treated cells followed by 980 nm light irradiation, while strong green fluorescence was found after 655 nm light treatment, suggesting the ROS was generated through BODIPY-mediated PDT by 655 nm light but not 980 nm. Meanwhile, dual light irradiation group (L_{980}+L_{655}) showed stronger green fluorescence than L_{655} group, indicating that photo-crosslinking of **DBNC-NPs** could enhance the release of

singlet oxygen. Sustainable releasing of singlet oxygen is crucial for enhanced PDT in the absence of light, which could be realized by the naphthalene unit acting as a singlet oxygen carrier. Under PDT, naphthalene could trap singlet oxygen to afford endoperoxide which re-releasing singlet oxygen *via* a cycloreversion reaction acting as "afterglow" therapy [38]. To confirm the "afterglow" release of singlet oxygen, MCF-7 cells were treated with **DBNC-NPs** and **DBC-NPs** (without naphthalene) followed 655 nm light irradiation. As shown in Fig. 2g and Fig. S11 (Supporting information), both **DBNC-NPs** and **DBC-NPs** could immediately release ROS under 655 nm light irradiation. Interestingly, **DBNC-NPs** treated group could persistently release ROS after 2 h while no ROS was detected in **DBC-NPs** group, suggesting that naphthalene worked as singlet oxygen carrier and was able to deliver singlet oxygen in the dark.

As many endoperoxides can liberate triplet oxygen in addition to singlet oxygen, we supposed that the *in situ* generated endoperoxides in **DBNC-NPs** could not only directly exert cytotoxic effects through singlet oxygen, but also release triplet oxygen for alleviating tumor hypoxia aggravated by PDT [39]. To assess the release of triplet oxygen, tetramethylethylene [40], a singlet oxygen probe was incubated with naphthalene endoperoxide. By integrating the specific peaks of the generated hydroperoxide and naphthene in the ^{1}H nuclear magnetic resonance (NMR) spectra, we were able to determine that approximately 82 % singlet oxygen and 18 % triplet oxygen were released simultaneously (Fig. S12 in Supporting information). Inspired by this finding, we evaluated the regulating ability of **DBNC-NPs**-mediated PDT on HIF-1α [41], a critical marker of cellular response under hypoxia condition. As depicted in Figs. 2h and i, Western blot analysis of MCF-7 cells under hypoxic conditions revealed that the accumulation of HIF-1α was markedly reduced by **DBNC-NPs** compared to **DBC-NPs** without singlet oxygen carrier, successfully demonstrating the role of triplet oxygen on the hypoxia relief [42]. Taken together, many evidences confirmed that **DBNC-NPs** nanodrug designed in this work showed long-acting capability by photoinduced-immobilization *via* crosslinking, and it features enhanced and sustainable anticancer ability *via* "afterglow" singlet oxygen release, hypoxia relief by triplet oxygen and ROS-triggered CPT release.

To evaluate the long-acting benefit for reducing the administration frequency, MCF-7 cells were incubated with **DBNC-NPs** for 8 h and was then irradiated by NIR light for drug immobilization. The cells were subsequently irradiated with 655 nm light for photodynamic therapy at 4-h intervals and MTT assays were carried out (Fig. 3a). Interestingly, multiple irradiations by 655 nm light lead to high cytotoxicity (IC_{50}, 4.6 μg/mL for three times, while 11.6 and 8.0 μg/mL for one and two times of 655 nm light irradiation, respectively), indicating the advantages driven from long-acting property of our nanodrug. The cytotoxicity of the **DBNC-NPs** toward other cancer cells (4T1, A549 and HeLa cells) were examined (Fig. 3b), and concentration-, laser density-dependent cytotoxicity were found as well (Fig. S13 in Supporting information). Non-tumorigenic cell lines NIH/3T3 and human umbilical vein endothelial cells (HUVEC) were tested and negligible cytotoxicity was observed (Fig. S14 in Supporting information), indicating the good safety of **DBNC-NPs**.

To verify the cellular uptake and intracellular localization of **DBNC-NPs**, MCF-7 cells were incubated with **DBNC-NPs** and various commercially available organelle-targeting dyes including ER-Tracker, Mito-Tracker, and Lyso-Tracker. As shown in Fig. 3c, the red fluorescence from **DBNC-NPs** overlapped well with the green fluorescence from the Lyso-Tracker and their co-localization coefficients was calculated to be 0.81. In contrast, poor correlation coefficients (0.6 and 0.52) were found from ER-Tracker and Mito-Tracker treated groups. These results suggested that **DBNC-NPs** were internalized to cell and localized in lysosomes specifically [43]. We also investigated the cell apoptosis and death pathways

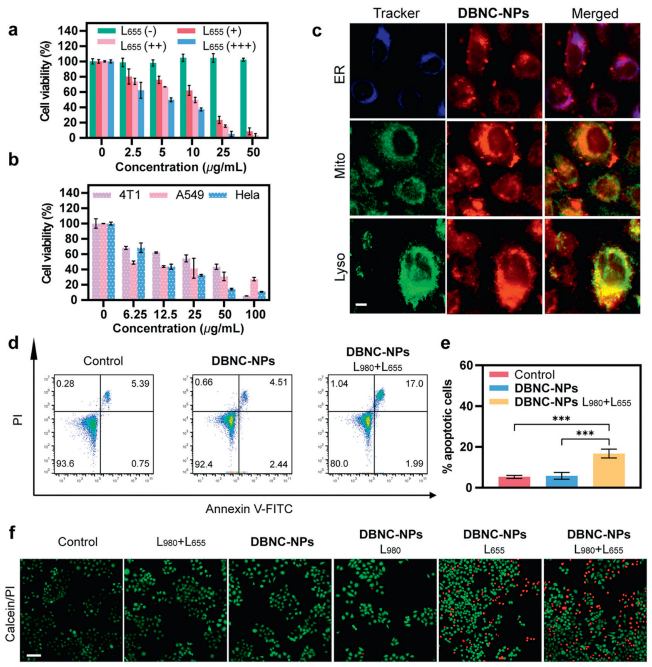


Fig. 3. (a) Viability of **DBNC-NPs** treated MCF-7 cells under 980 nm light and then multiple 655 nm light irradiation. (b) Cell viability of 4T1, A549 and HeLa cells incubated with **DBNC-NPs** at various concentrations after 980 nm light (3 W/cm^2, 4 min) and then 655 nm light (10 mW/cm^2, 20 min) irradiation. (c) Fluorescent images of MCF-7 cells stained with **DBNC-NPs** and various organelle-targeting dyes. Scale bars: 10 μm. (d, e) Apoptotic rates of MCF-7 cells with various treatments by flow cytometry. (f) Live and dead assay of MCF-7 cells stained with calcein-AM (green) and PI (red). Scale bar: 100 μm. Data are shown as mean ± SD ($n = 3$). $^{***}P < 0.001$.

induced by **DBNC-NPs** (Figs. 3d and e). In the control groups, where cells were treated with **DBNC-NPs** without light exposure, the survival rate remained high at approximately 94 %, with no significant apoptosis signals detected. However, the percentage of apoptotic cells increased markedly to 17 % upon exposure to 980 and 655 nm light irradiation, indicating that **DBNC-NPs**-mediated PDT can effectively trigger the apoptosis of tumor cells. To visually evaluate the *in vitro* therapeutic effect, the cells were stained with calcein acetoxymethylester (calcein-AM) and propidium iodide (PI) to identify live and dead/late apoptotic cells. As can be seen from Fig. 3f and Fig. S15 (Supporting information), MCF-7 cells incubated with **DBNC-NPs** after 980 nm and 655 nm light irradiation displayed stronger red fluorescence than other groups, demonstrating that **DBNC-NPs**-mediated PDT could effectively kill tumor cells which was further enhanced by 980 nm light induced immobilization. Collectively, these results validated the efficient therapeutic effect enabled by the NIR light-triggered long-acting nanodrugs *via* enhanced and sustainable photodynamic and chemo-therapy.

Before conducting the *in vivo* antitumor evaluation of **DBNC-NPs**, we first assessed their tumor accumulation and retention effect using 4T1 tumor-bearing mice as the model. All animal studies were approved by the Ethics Committee of the Dalian University of Technology (No. DUTSCE240626–01). When the tumor volume reached ~100 mm^3, mice were intravenously injected with **DBNC-NPs** and monitored by normalized fluorescence imaging. As shown in Figs. S16 and S17 (Supporting information), the onset of red fluorescence of **DBNC-NPs** was observed at the tumor site after 2 h post-injection, and the fluorescence intensity unceasingly increased over time which reaching the highest accumulation at 24 h. After this, the fluorescence intensity of **DBNC-NPs** began to decline, indicating a reasonable but limited retention time in tumor site. In contrast, **DBNC-NPs** under NIR light irradiation at 24 h showed

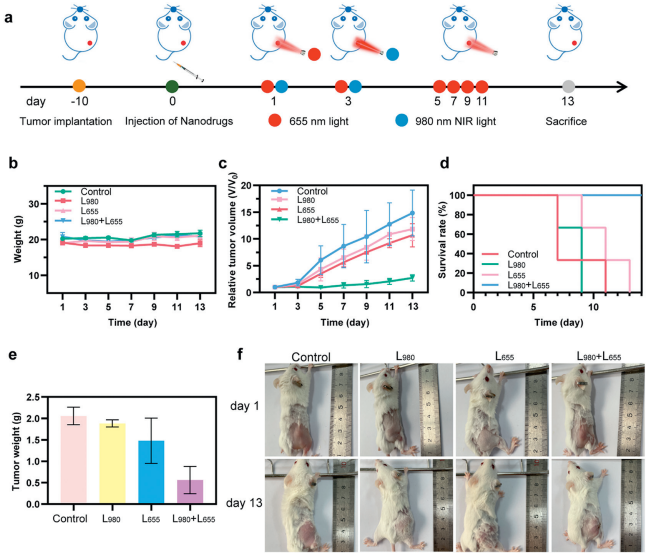


Fig. 4. (a) Schematic illustration of *in vivo* antitumor evaluation. (b) Changes in body weight of mice under various treatments. (c) Relative tumor volume of mice under various treatments. (d) The survival curves of mice in different groups, which was calculated based on whether the tumor volume reached to 1000 mm^3. (e) Tumor weight of mice under various treatments. Data are presented as mean ± SD ($n = 3$). (f) Representative 4T1 tumor-bearing mice under various treatments on day 1 and day 13, respectively.

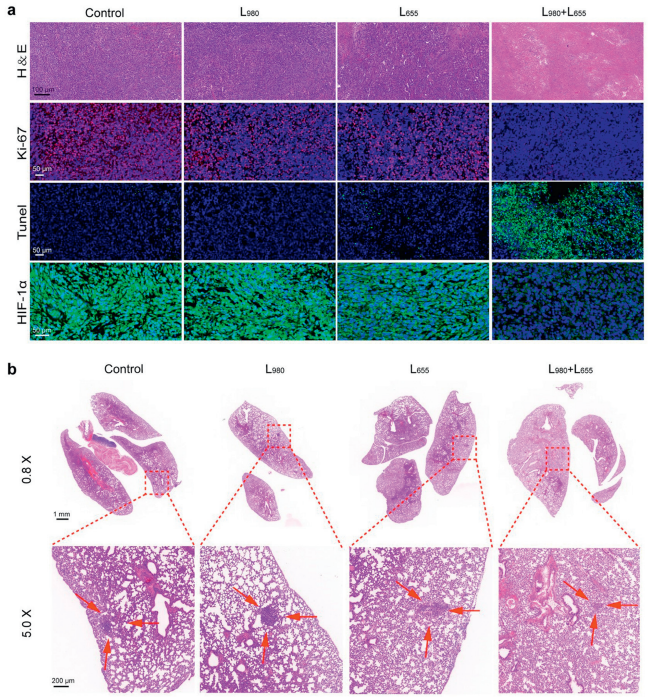


Fig. 5. (a) H&E and immunofluorescence staining of Ki-67, TUNEL and HIF-1α in 4T1 tumor sections of mice under various treatments. (b) Representative H&E staining of the lungs from mice under different treatments for 13 days. The scales for full (up) and enlarged (down) images are 1 mm and 200 μm, respectively.

enhanced tumor retention and strong red fluorescence was found even after 240 h injection, which was possibly caused by the drug immobilization *via* NIR light-induced photo-crosslinking.

To further confirm the enhanced retention of **DBNC-NPs** under 980 nm light irradiation, we established two tumor-bearing mice model which were intratumorally injected with **DBNC-NPs** in two sites, respectively. As shown in Fig. S17, two tumor site both emitted strong fluorescence at 0 h time point, but enhanced retention was easily observed in the right tumor (irradiated by 980 nm light), suggesting the enhanced retention capacity of **DBNC-NPs** induced by NIR light. *Ex vivo* fluorescence imaging of the tumor and major organs offered further insights into the tumor-targeting efficiency and retention behavior of **DBNC-NPs**, and the results showed that **DBNC-NPs** accumulated and immobilized well in the right tumor under 980 nm light irradiation (Fig. S18 in Supporting information). In addition, two tumor-bearing mice intravenously injected with **DBNC-NPs** were irradiated with 980 nm light after 24 h post-injection and consist results were observed (Fig. S19 in Supporting information). It was revealed that **DBNC-NPs** displays good tumor accumulation *in vivo* and its retention time could be significantly prolonged by the NIR light-mediated crosslinking.

Encouraged by the excellent tumor accumulation and enhanced photo-induced retention *in vivo*, we started to evaluate the antitumor activity of **DBNC-NPs** using 4T1 tumor-bearing mice which were randomly divided into four groups for different treatments (Fig. 4a). Mice in control group were intravenously injected with saline and other groups were intravenously injected with **DBNC-NPs**. Give the credit to the excellent retention time of **DBNC-NPs** under 980 nm light irradiation (up to 10 days), all mice were treated with one dosage of **DBNC-NPs** (3 mg/mL, 300 μL) during the entire treatment process. Mice in the therapeutic group were exposed to 655 nm light (11 mW/cm^2) for PDT and 980 nm light (3.5 W/cm^2) for immobilization (L_{980}+L_{655}) on day 1 and day 3. After day 5, 655 nm light-mediated PDT was performed at every other day. Mice in the groups indicated as L_{980} or L_{655} were irradiated with the corresponding light source. Throughout two weeks treatment, we recorded the tumor volume and body weight of each mouse. As shown in Fig. 4b, all mice maintained their body weight and exhibited normal behavior, indicating the high biocompatibility of **DBNC-NPs**. On day 13, the mice were sacrificed for further analysis. The relative tumor volume of mice was plotted and the L_{980} group displayed similar growth curves compared to the saline group (Fig. 4c). Mice in L_{655} group showed slight inhibition for tumor growth, but significant inhibition of tumor growth (84 %) was observed in the mice irradiated by both 655 nm and 980 nm light (L_{980}+L_{655}), indicating the enhanced and sustainable anticancer effect of **DBNC-NPs** caused by multiple functions. The survival curve was calculated based on whether the tumor volume reached to 1000 mm^3, and the results strongly revealed the therapeutic potential of **DBNC-NPs** (Fig. 4d). In addition, tumor weight in L_{980}+L_{655} was decreased by 73 % compared to that in control group, suggesting the excellent tumor inhibition potential of **DBNC-NPs** *in vivo* (Figs. 4e and f, Figs. S20–S22 in Supporting information).

The histological analysis was performed on tumor tissues stained with hematoxylin and eosin (H&E), Ki-67 and TdT-mediated dUTP nick-end labeling (TUNEL) staining (Fig. 5a). In the control and L_{980} groups, the cellular morphology remained intact. In contrast, the L_{655} group exhibited disintegrated nuclei and severe tissue necrosis. As expected, significant higher damages were observed in L_{980}+L_{655} group, indicating its good anticancer performance. The hypoxia relief ability of **DBNC-NPs** was also studied *in vivo*. Immunofluorescence analysis of HIF-1α levels in tumor tissues indicated that L_{980}+L_{655} group significantly reduced HIF-1α protein levels thereby alleviating hypoxia in the mice, suggesting that **DBNC-NPs** effectively improves the hypoxic conditions within the tumor microenvironment (Fig. 5a and Fig. S23 in Supporting information). The superior therapeutic efficacy of **DBNC-NPs** encouraged us to evaluate their suppressive effect on tumor metastasis, which is a common occurrence in breast cancer patients [44]. To study cancer metastasis during treatment, we performed H&E staining analysis on lung tissue of mice after 13

days treatment (Fig. 5b). Remarkable metastatic lesions were observed in all treatment groups except for the group receiving the 980 and 655 nm light exposure (L_{980}+L_{655}, Fig. 5b, upper). Extensive metastatic lesions with agminated nuclei were confirmed microscopically (Fig. 5b, lower), which demonstrated the excellent capacity of the **DBNC-NPs** to impede tumor metastasis. To assess the *in vivo* biocompatibility of **DBNC-NPs**, major organs and blood samples in all groups were harvested for hematological and histological examinations. Blood analysis also revealed the good biocompatibility of **DBNC-NPs** and H&E staining of major tissues showed no significant pathological damage in all groups (Fig. S24 in Supporting information).

In summary, we developed a potential anticancer nanodrug which is capable of reducing the frequency of administration and overall drug dosage by controlled prolonging the retention time of photosensitizers in tumor tissues *via* NIR light-induced crosslinking. It not only addresses the challenges of hypoxia induced by traditional PDT, but enhances anticancer efficacy by persistently delivering singlet oxygen in the dark and provides synergistic treatments through PDT and CPT-mediated chemotherapy. It is discovered for the first time that hypoxia relief was achieved by photosensitizer/endoperoxide combination. This light triggered long-acting strategy offers advantages of the spatio-temporal regulation ability, enabling a more efficient therapeutic effect and safety. *In vitro* imaging and proteins immobilization revealed that this nanodrug exhibited enhanced retention time through carbenes-mediated crosslinking *via* a upconversion process, and demonstrated remarkable phototoxicity against cancer cells which was attributed by the persistent release of singlet oxygen and the synergistic treatments involving PDT and CPT. Meanwhile, cellular experiments successfully demonstrated that endoperoxide generated *in situ* could downregulate the expression of hypoxia marker HIF-1α. *In vivo* imaging work showed that it demonstrated exceptional tumor targeting specificity, high accumulation and prolonged retention. Most importantly, this nanodrug exhibits excellent *in vivo* anticancer activity with only a single administration, effectively inhibiting tumor growth, alleviating hypoxia, suppressing tumor metastasis and demonstrating good biosafety. This strategy provides an available and facile approach to break down the barriers to photodynamic therapy and multidrug resistant, and could be used for long-term imaging [45,46] in cancer diagnosis in the future.

Declaration of competing interest

The authors declare that they have no known competing financial interests or personal relationships that could have appeared to influence the work reported in this paper.

CRediT authorship contribution statement

Yu Si: Writing – original draft, Methodology, Data curation. **Xueying Jiang:** Data curation. **Zhigang Gao:** Methodology. **Yuan Liang:** Methodology, Conceptualization. **Wen Sun:** Methodology. **Engin U. Akkaya:** Methodology. **Lei Wang:** Writing – original draft, Project administration, Methodology, Investigation, Funding acquisition, Conceptualization.

Acknowledgments

This work was supported by the National Natural Science Foundation of China (No. 22007008), the LiaoNing Revitalization Talents Program (No. XLYC1907021) and the Fundamental Research Funds for the Central Universities (Nos. DUT23YG120, DUT19RC (3)009).

Supplementary materials

Supplementary material associated with this article can be found, in the online version, at doi:10.1016/j.cclet.2025.111195.

References

[1] Y. Qin, M. Huang, C. Huang, et al., Chin. Chem. Lett. 35 (2024) 109171.
[2] B. Yin, X. Liu, Z. Li, et al., Chin. Chem. Lett. 36 (2025) 110119.
[3] R. Langer, D. Peer, J.M. Karp, et al., Nat. Nanotech. 2 (2007) 751–760.
[4] X. Li, S. Lee, J. Yoon, Chem. Soc. Rev. 47 (2018) 1174–1188.
[5] R. Wang, M. He, Z. Zhang, et al., Smart Mol. 2 (2024) e20240010.
[6] S. Mura, J. Nicolas, P. Couvreur, Nat. Mater. 12 (2013) 991–1003.
[7] T.C. Pham, V.N. Nguyen, Y. Choi, S. Lee, J. Yoon, Chem. Rev. 121 (2021) 13454–13619.
[8] Z. Zhao, T. Chen, J. Li, et al., Smart Mol. 3 (2025) e20240049.
[9] J.N. Liu, W. Bu, J. Shi, Chem. Rev. 117 (2017) 6160–6224.
[10] B. Zhang, L. Lin, J. Mao, et al., Chin. Chem. Lett. 34 (2023) 108518.
[11] E.B. Rankin, A.J. Giaccia, Science 352 (2016) 175–180.
[12] X. Song, L. Feng, C. Liang, K. Yang, Z. Liu, Nano Lett. 16 (2016) 6145–6153.
[13] T. Liang, B. Zhang, Z. Xing, et al., Angew. Chem. Int. Ed. 60 (2021) 11464–11473.
[14] J. Kim, H.R. Cho, H. Jeon, et al., J. Am. Chem. Soc. 139 (2017) 10992–10995.
[15] G. Yang, L. Xu, Y. Chao, et al., Nat. Commun. 8 (2017) 902.
[16] H. Wu, L. Wang, Y. Wang, et al., Angew. Chem. Int. Ed. 134 (2022) e202210249.
[17] L. Wang, L. Tang, Y. Liu, et al., Chem. Commun. 58 (2022) 1902–1905.
[18] L. Wang, H. Wu, Z. Liu, et al., Angew. Chem. Int. Ed. 63 (2024) e202408473.
[19] G. Li, R. Zhou, W. Zhao, et al., Research 2020 (2020) 5351848.
[20] S. Kuang, F. Wei, J. Karges, et al., J. Am. Chem. Soc. 144 (2022) 4091–4101.
[21] W. Xiao, P. Wang, C. Ou, et al., Biomaterials 183 (2018) 1–9.
[22] W. Fudickar, T. Linker, Angew. Chem. Int. Ed. 57 (2018) 12971–12975.
[23] J. Das, Chem. Rev. 111 (2011) 4405–4417.
[24] L. Wang, A. Ishida, Y. Hashidoko, M. Hashimoto, Angew. Chem. Int. Ed. 56 (2017) 870–873.
[25] J.B. Geri, J.V. Oakley, T. Reyes-Robles, et al., Science 367 (2020) 1091–1097.
[26] M. Hashimoto, Y. Hatanaka, Eur. J. Org. Chem. 2008 (2008) 2513–2523.
[27] P. Kleiner, W. Heydenreuter, M. Stahl, V.S. Korotkov, S.A. Sieber, Angew. Chem. Int. Ed. 56 (2017) 1396–1401.
[28] C. Ash, M. Dubec, K. Donne, T. Bashford, Laser Med. Sci. 32 (2017) 1909–1918.
[29] Y. Yang, Y. Chen, P. Pei, et al., Nat. Nanotech. 18 (2023) 1195–1204.
[30] T. Wang, S. Wang, Z. Liu, et al., Nat. Mater. 20 (2021) 1571–1578.
[31] S.L. Zhang, P. Liu, L. Li, et al., ACS Appl. Mater. Interfaces 15 (2023) 40280–40291.
[32] R.K. Jain, T. Stylianopoulos, Nat. Rev. Clin. Oncol. 7 (2010) 653–664.
[33] A. Banstola, K. Poudel, S. Pathak, et al., ACS Appl. Mater. Interfaces 13 (2021) 22955–22969.
[34] L.M. Herda, D.R. Hristov, M.C. Lo Giudice, E. Polo, K.A. Dawson, J. Am. Chem. Soc. 139 (2017) 111–114.
[35] K. Abstiens, M. Gregoritza, A.M. Goepferich, ACS Appl. Mater. Interfaces 11 (2019) 1311–1320.
[36] A. Kamkaew, S.H. Lim, H.B. Lee, et al., Chem. Soc. Rev. 42 (2013) 77–88.
[37] J. Tian, B. Li, C. Wu, et al., J. Am. Chem. Soc. 146 (2024) 16458–16468.
[38] J. Zou, L. Li, J. Zhu, et al., Adv. Mater. 33 (2021) 2103627.
[39] X. Li, N. Kwon, T. Guo, Z. Liu, J. Yoon, Angew. Chem. Int. Ed. 57 (2018) 11522–11531.
[40] M. Matsumoto, M. Yamada, N. Watanabe, Chem. Commun. (2005) 483–485.
[41] D.M. Livingston, A.L. Kung, S. Wang, J.M. Klco, W.G. Kaelin, Nat. Med. 6 (2000) 1335–1340.
[42] X. Liang, M. Chen, P. Bhattarai, S. Hameed, Z. Dai, ACS Nano 14 (2020) 13569–13583.
[43] D.M. Xi, N. Xu, X. Xia, et al., Adv. Mater. 34 (2022) 2106797.
[44] D. Huang, Y. Zou, H. Huang, et al., Adv. Mater. 36 (2024) 2313460.
[45] S. Skylaki, O. Hilsenbeck, T. Schroeder, Nat. Biotechnol. 34 (2016) 1137–1144.
[46] Y. Zhang, X. Lv, Y. Wang, et al., Smart Mol. 2 (2024) e20240031.